where γ_0 is the propagation constant for the free guide. Eq. (25) may be simplified to

$$R = R_0\left[\frac{1 - (j\gamma_s\alpha_2 e^{-t/\tau})/(\gamma_0 - \gamma_s)}{1 + (j\gamma_s\alpha_2 e^{-t/\tau})/(\gamma_0 + \gamma_s)}\right] \quad (27)$$

where R_0 is the reflection coefficient before modulation.

The first-order approximation of R is

$$R = R_0[1 - (2j\gamma_0\gamma_s\alpha_2 e^{-t/\tau})/(\gamma_0^2 - \gamma_s^2)]. \quad (28)$$

Evidently then the information relating to lifetime may also be obtained by observing the reflected signal only.[7] It should, however, be noted that due to the increased carrier density both the magnitude and phase of reflection is changed. Hence, the change in the magnitude of the reflected signal will have the wave shape of the modulation only if it is observed alone. If the detected signal is due to the combination of both the incident and reflected signal, the wave shape may be very different.

On the other hand, if the transmitted signal is observed by locating a probe inside the semiconductor or by a matched detector, the observations made in the previous section are mostly applicable, only the amplitude is multiplied by the factor T. The effect of the change in carrier density on the value of T may be considered to be small. It will be more so in the logarithmic display, as suggested earlier.

[7] S. Deb and B. R. Nag, "Measurement of lifetime of carriers in semiconductors through microwave reflection," *J. Appl. Phys.*, vol. 33, p. 1604; April, 1962.

Conclusion

Expressions have been obtained for electromagnetic fields propagating in a waveguide filled with a semiconductor with carrier density varying with time. It has been shown that due to the variation of carrier density both the amplitude and phase modulation occur. The phase modulation reproduces the wave shape correctly. The wave shape of amplitude modulation is correct only for small attenuation. However, the logarithm of the amplitude reproduces the wave shape correctly even for larger attenuation.

It has also been shown that the reflected signal from a semiconductor surface may be used to measure the lifetime. The effect of reflection on the wave shape of the transmitted signal is also found to be small.

Acknowledgment

The authors are indebted to Prof. J. N. Bhar for his kind supervision of the work.

On the Resonant-Cavity Method for Measurement of Varactors*

FRANK KEYWELL†

Summary—An extension of Houlding's method for measurement of varactor quality has been developed by using a swept-bias voltage instead of a discrete step in bias. The method can be used to measure the cutoff frequency of high-Q varactors if the law of capacitance variation is known. In this case, it is not necessary to measure capacity or reactance since cutoff frequency is shown to be determined by reflected power on a microwave-reflectometer system. The Sweep-Voltage Method places emphasis on the measurement of reflected power and a test bench is described for application of the method.

The series resistance of high-voltage epitaxial varactors is shown, by calculation and experimental data, to be a function of bias. This is due to space-charge layer widening which causes the epitaxial base layer to vary in length. For this reason it is advantageous to compare high-voltage epitaxial varactors by sweeping the bias over a broad range of the diode characteristics. Data is given for typical per cent of reflected microwave power $\tilde{R}$ for 6.5-, 15-, and 100-v varactors where the varactor is matched to the line at 2.00-, 5.00- and 15.0-v bias and a sine wave at 100 kc with amplitude 4.00, 10.0 or 30.0 v is superimposed on the bias. The measurements are independent of the power incident on the varactor to a level of 700 μw.

I. Introduction

THE QUALITY of a microwave varactor diode is related to the losses in and near the p-n junction which provides the voltage-variable reactance. These losses are accepted to be equivalent to a constant resistance R_s in series with a voltage-variable capacitance. A method for measurement of R_s has been described by Houlding[1] wherein the varactor is in a

* Received May 2, 1962; revised manuscript received July 11, 1962.

† Semiconductor Devices Inc., Newport Beach, Calif.

[1] N. Houlding, "Measurement of varactor quality," *The Microwave J.*, p. 40; January, 1960.

matched resonant cavity and the VSWR due to a step in varactor bias provides a measure of R_s. This paper will describe an extension of the resonant-cavity method wherein a sweeping bias is applied to the varactor instead of a single step in bias.

The present method for measuring R_s will be termed the Sweep-Voltage Method (SVM) as compared with the Single-Point Method (SPM) originally described by Houlding. It will be assumed the reader is familiar with the Single-Point Method and the advantages of making the measurements with a resonant system. In particular, Houlding described a technique for using the SPM without making capacitance measurements if the law of capacitance variation of the varactor is known. The Sweep-Voltage Method is basically an extension of this technique. The varactor is placed in a cavity and matched at a suitable bias point to incident microwave power; then a known periodic sweeping voltage at low frequency is applied to it to produce a measurable reflected wave. The magnitude of the average reflected power is a direct measure of varactor cutoff frequency provided the law of capacitance variation is known. The SVM has the following advantages:

1) CW power is measured rather than VSWR.
2) Capacitance or reactance measurements are not required.
3) It is rapid and reliable.
4) The measurement can be made at power level to the order of 1 mw.
5) Comparison can be made of the average cutoff frequency of high-voltage epitaxial varactors.

Characteristics 1) to 5) are also common with the SPM when the law of capacitance variation is known; 4) and 5), however, are properties where the SVM provides an improvement in the technique of measurement.

The SVM, as applied to varactors for parametric amplifiers, has the disadvantage mentioned above of requiring knowledge of the law of capacitance variation. The difficulty is overcome by the knowledge that, for high-Q diffused silicon mesa varactors, the familiar inverse cube-root law of capacitance variation is closely satisfied with a built-in potential of 0.6 v. On the other hand, high-voltage epitaxial varactors do not have a fixed R_s, as will be discussed in Section II, hence a defined measurement of their cutoff frequency by the SVM is not meaningful. Nevertheless, the SVM provides a useful means for determining the *average reflection* due to a given varactor under a *fixed set of conditions*, consequently an accurate comparison of high-voltage epitaxial varactors may be made by this technique.

The SVM has applications therefore to both high-Q varactors for parametric amplifiers and high-voltage epitaxial varactors. The manner of application has a wide variety of possibilities since the waveform and bias applied to the varactor are arbitrary. The present paper will describe measurements made with application of a sine wave of peak-to-peak amplitude of twice the bias voltage. Furthermore, the measurements were made specifically on diffused silicon mesa varactors, namely high-Q and high-voltage epitaxial varactors (HIVEV). This encompasses a large class of varactors which have provided outstanding performance in Parametric Amplifiers and Harmonic Generators.[2] A discussion of the characteristics of HIVEV will be presented in relation to the application of the SVM to their measurement.

II. Measurement by the Sweep-Voltage Method

A. Theory of Measurement

The measurement of varactor series resistance is related to reactance and Q through the relation $Q=X_c/R_s$. There are advantages in beginning with the differential relation $\Delta Q=\Delta X_c/R_s$ which is most readily applied to the resonant method. The series resistance must be measured at microwave frequency to include dielectric losses in the p-n junction in addition to the ohmic losses adjacent to the junction. The reactance change due to the controlled bias voltage applied to the varactor is readily determined from capacitance measurements made on a low-frequency bridge. Consequently, the measurement of R_s by Houlding's resonant method is essentially the determination of ΔQ at microwave frequency. This statement is equivalent to the following: the measurement of R_s by Houlding's resonant method is essentially the measure of reflected power of a signal at fixed frequency from a tuned resonant cavity due to controlled bias voltage applied to a varactor in the cavity. We are thus led to conclude that *reflected power, with all bias conditions held fixed*, is a *fundamental variable* in evaluating or comparing the quality of varactors. Reflected power, on the other hand, should not be construed to replace cutoff frequency as a figure of merit.

The basic nature of reflected power in the measurement of R_s is emphasized by noting that its measurement is necessary in all variations of the method described by Houlding. Reactance measurements, on the other hand, were capable of substitution by controlled bias voltage if the law of capacitance variation was known. Continuing with this emphasis on reflected power, we will presently consider the method for measuring R_s by means of a sweeping voltage applied to the varactor; the average reflected power due to this sweeping voltage is a direct measure of at least one factor related to quality of the varactor.

One might be inclined to question the advantage of applying a swept bias to the varactor since the method appears to be merely a variation of the SPM. It devel-

[2] R. D. Weglein and F. Keywell, "A low noise X-band parametric amplifier using a silicon mesa diode," IRE Trans. on Microwave Theory and Techniques, vol. MTT-9, pp. 39–43; January, 1961.

ops in practice however that, in addition to its convenience, a swept bias will provide a reliable comparison of the quality of high-voltage epitaxial varactors under conditions where the SPM gives ambiguous results due to the variation in R_s with bias voltage. The SVM derives an advantage from the principle that an average reflection due to the bias voltage being swept over a wide range provides the most reliable comparison of the average reactive variation due to applied bias in relation to average losses.

The principles of application of the SVM are a straightforward extension of the resonant method. Consider a varactor with a capacitance-voltage dependence of the form shown in Fig. 1. When the varactor is reverse-biased to a mean value of voltage V_B and a sinusoidal voltage V_B sin $2\pi f_s t$ is superimposed on V_B, there will be a variation in capacitance with time of the form indicated in Fig. 1. The sweeping frequency f_s can be chosen at a suitable low frequency. The capacitive reactance of the varactor at microwave frequency will be $X_c(t) = 1/2\pi f_m C(t)$ and its variation with time will also be of the form indicated in Fig. 1. Now, if the varactor is mounted in a cavity and matched at V_B to microwave energy at frequency f_m while its bias voltage is swept with V_B sin $2\pi f_s t$, there will be a periodic mismatch of the resonant cavity to the incident microwave energy. The energy reflected from the cavity due to this mismatch is directly related to the quality of the varactor due to the dependence of VSWR on the ratio $\Delta X_c/R_s$.[1]

In the special case of high-Q silicon mesa varactors for Parametric Amplifiers (breakdown voltage$\simeq$6.5 v), the series resistance is effectively constant. This results from the p-n junction for this type of varactor having been formed in low-resistivity silicon, hence its width does not vary appreciably with application of bias voltage. Additionally, the law of capacitance variation follows the familiar inverse cube-root law with built-in potential of 0.6 v for representative high quality varactors. Assuming the varactor equivalent to a constant resistance R_s in series with a voltage-variable capacitance of the form $C(V) = C_0(1 + V/\phi)^{-1/3}$, consider the varactor biased at V_B and matched to a waveguide for a CW microwave at known power and frequency. Application of a sinusoidal voltage $v = V_B$ sin $2\pi f_s t$ will result in a capacity variation of the form

$$C = \frac{C_0}{\left(1 + \dfrac{V_B(1 + \sin 2\pi f_s t)}{0.6}\right)^{1/3}}.$$

This variation in capacitance will result in calculable reactance mismatch at every instant of time over a complete cycle, hence a wave of instantaneous power reflected as a function of $\theta = 2\pi f_s t$ can be calculated for any assumed value of R_s. The calculated average power reflected, $\tilde{R}$, is obtained from the relation by numerical integration of the R vs θ curve. In order to calculate a

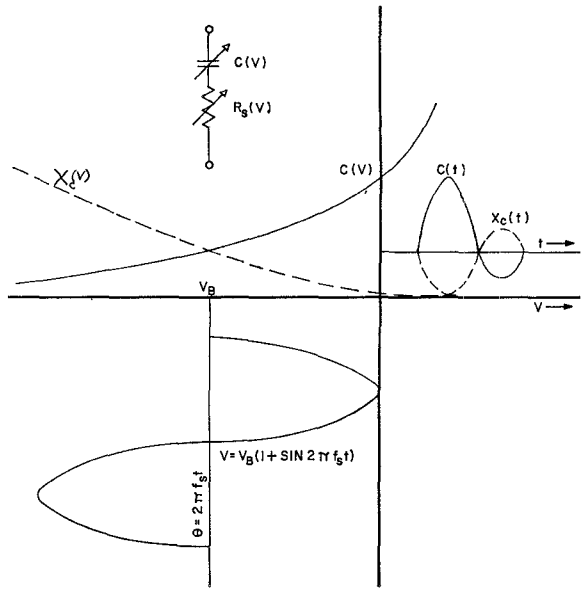

Fig. 1—Capacitance and reactance vs swept-bias voltage.

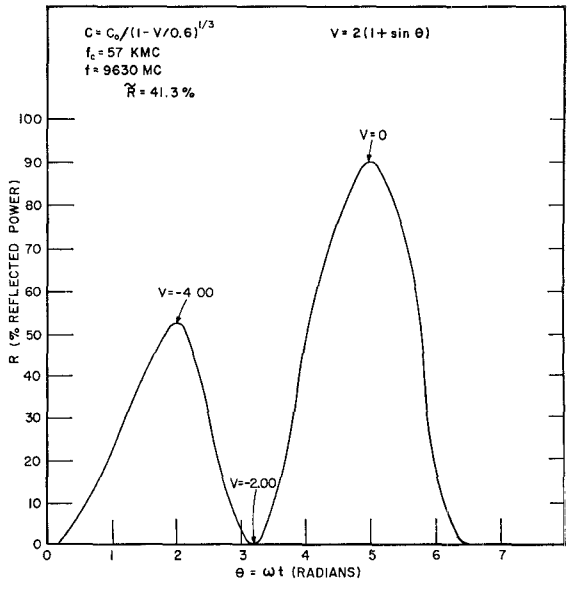

Fig. 2—Per cent reflected power vs phase ($\theta = 2\pi f_s t$).

calibration curve of $\tilde{R}$ vs f_c, initially choose a set of values for R_s, $C(0)$, and $f_c = 1/2\pi R_s C(0)$. Next, with equal increments in θ over zero to 2π, calculate the following values in tabular form:

$$\theta,\ v = V_B(1 + \sin\theta), \quad C(v) = C(0)/(1 + v/0.6)^{1/3},$$
$$X_c(v) = 1/2\pi f_m C(v);$$

ΔX_c, $\Delta X_c/R_s$, VSWR and R. ΔX_c is considered relative to a matched condition at V_B. VSWR is read by striking a radius on a Smith Chart from $\Delta X_c/R_s$ on the Unit Circle to the VSWR line on the chart. A typical curve of R vs θ for a 57 kMc varactor is shown in Fig. 2 where the reflected power is R in per cent of incident power.

The reflected power R is independent of zero bias capacity for varactors with the same cutoff frequency. This important property is apparent from the following considerations: If the capacity is increased by k, then X_c and ΔX_c are similarly decreased by the factor k. The series resistance R_s is also decreased by k since cutoff frequency is constant. Therefore, $\Delta X_c/R_s$ is constant and the curve of R vs θ is independent of capacitance at zero bias but it is uniquely determined by the cutoff frequency at zero bias.

In practice, we can now apply Houlding's Resonant Method in the following manner:

1) Tune out the varactor with 2.00-v reverse bias and an X-band signal of known power and frequency incident on the diode.
2) Superimpose on the bias voltage a 4.00-v peak-to-peak sinusoidal signal at low frequency and measure the average per cent reflected power $\tilde{R}$.
3) Read the varactor cutoff frequency from a curve of $\tilde{R}$ vs f_c.

It is not necessary to measure capacitance or reactance change since $\tilde{R}$ is directly related to f_c, independent of capacitance. R_s can be calculated, if required, by means of a capacitance measurement and the relation $R_s = 1/2\pi f_c(0)C(0)$.

B. Experimental

The test bench, Fig. 3, was set up with a signal generator at 9630-Mc and 200-μw available power into a matched load (see Appendix). The signal passed through a 3-db directional coupler and a slotted line followed by a waveguide short before it reached the "cavity" consisting of an E-H tuner and diode mount with a sliding short. Tuning of the cavity was accomplished by observing the reflected wave with the spectrum analyzer. The varactor was biased at 2.00-v reverse and matched to the line by using the E-H tuner and sliding short to minimize the reflected wave. A 4.00-v peak-to-peak signal at 100 kc was then applied to the varactor and the reflected energy was switched to the power meter. Calculations of average per cent reflected power $\tilde{R}$ for a frequency of 9630 Mc, give the relation between $\tilde{R}$ and $f_c(0)$ as

$$f_c(0) = 1.33\tilde{R} + 4 \text{ [kMc]}$$
$$25 \text{ per cent} < \tilde{R} < 60 \text{ per cent}$$

to accuracy of 1.5 per cent over the range of $\tilde{R}$.

The error due to small random deviation of the built-in potential from 0.6 v is not great as shown by a calculation of $\tilde{R}$ for a 57-kMc varactor with $\phi = 0.6$ or 0.5 v. The increase in $\tilde{R}$ due to change in ϕ from 0.6 to 0.5 v was from 41.3 per cent to 44.5 per cent. Table I shows a comparison of f_c determined by the SVM and the SPM for some typical varactors produced by Semiconductor Devices Incorporated. There is good agreement between the two methods over a considerable range of capacitance.

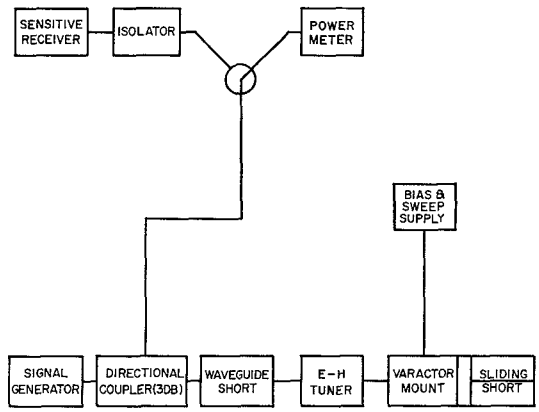

Fig. 3—Test bench.

TABLE I

COMPARISON BETWEEN CUTOFF FREQUENCY MEASURED BY SVM AND SPM FOR HIGH-Q VARACTORS

Diode No.	Capacitance @ zero bias ($\mu\mu$f)	$\tilde{R}$ (%)	$f_c(0)$* SVM (kMc)	$f_c(0)$† SPM (kMc)
SD-11-5A	0.360	40	57	58
SD-11-5B	0.562	40	57	55
SD-11-7C	0.892	50	70	71
SD-11-4D	1.783	34	49	51

Cutoff frequency at zero bias. 6.5-v breakdown varactors.
* 2.00-v bias—4.00-v peak-to-peak sine wave per 100 kc.
† Match at zero bias—1-v reverse bias for reactance change.

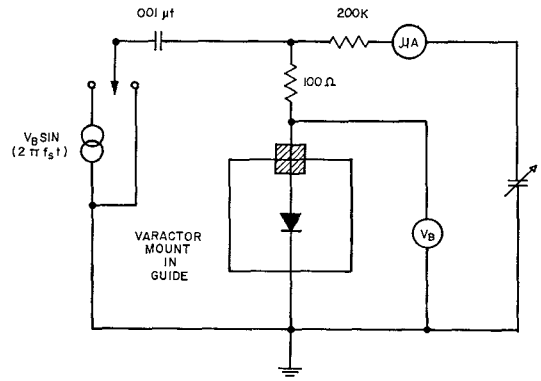

Fig. 4—Low-frequency sweep circuit.

A few remarks on the sweep arrangement and its use may be in order. The circuit was arranged as shown in Fig. 4. Amplitude of the sweep voltage was adjusted to equal the bias voltage and the sweep frequency was arbitrarily chosen to be 100 kc. The varactor was initially tuned with the input capacitor grounded and the bias set at V_B then the signal was switched onto the varactor to produce a reflected wave. The reflected power has been observed independent of frequency from 60–10^5 cps. The connections between the signal generator, the bias supply and the waveguide-detector mount were made by means of a small chassis which connected the components by standard fittings (BNC connectors, two-prong banana jacks, etc.).

C. High-Voltage Epitaxial Varactors, HIVEV

The present method SVM cannot be used to measure the cutoff frequency of high-voltage epitaxial varactors. This limitation is mainly a result of the dependence of series resistance on bias voltage. HIVEV are made by diffusion of impurities into a high-resistivity layer, the epitaxial layer, on a low-resistivity substrate wafer. The *p-n* junction formed in the epitaxial layer will have high breakdown voltage because of the increase in this parameter with increasing resistivity. The ohmic losses external to the *p-n* junction are a sum of the losses due to constriction resistance at the base of the mesa and ohmic resistance in the epitaxial material along the mesa. The variable capacitance of HIVEV is bought by varying the width of a space-charge region near the junction, hence the thickness of the epitaxial base layer varies with applied bias. This variation in the length of epitaxial base material along the mesa is of sufficient magnitude to cause a large variation in series resistance when voltage is applied to the *p-n* junction.

The effect of space-charge layer widening on R_s can be described in semiquantitative terms. Consider a *p-n* junction with 100-v breakdown formed at a depth of 11 microns in an epitaxial layer of 6-ohm-cm silicon 0.6 mil in thickness. The concentration gradient of impurities at the junction would be about 4×10^{19} cm^{-4}. The built-in potential for such a junction has been measured to be 0.4 v, hence, applying equations derived by Shockley,[3] the width of the space-charge region of the *p-n* junction at zero bias is 10^{-4} cm (0.04 mil). The width of the space-charge region can increase by a factor near ten since capacity may decrease by this factor on application of peak reverse bias. Thus $\frac{2}{3}$ of the epitaxial layer has been converted to space-charge region and the residual resistance in the neutral layer would be reduced to $\frac{1}{3}$ of its original value. Such an order of variation in resistance with bias is readily observed by means of measurements made by the resonant method.

The impedance of high-Q low breakdown voltage varactors measured by the SPM normalized for a match at zero bias will follow the Unit Circle on a Smith Chart.[1] Such is not the case for 100-v HIVEV where the plot of phase and VSWR due to bias yields a curve with significant deviations from the Unit Circle. Finally, the series resistance of HIVEV, when measured at separate bias points with a single point measurement, will vary by a factor as large as three to one. Consequently the cutoff frequency as a function of bias varies by more than the variation due to capacity alone. Typical data for these measurements is shown in Table II. It is apparent that rating of HIVEV by a cutoff frequency at high reverse voltage is misleading since the value of this quantity at or near zero bias may be reduced by a factor the order of thirty to one. It would seem desirable to quote cutoff frequency at both zero bias and breakdown voltage. A suitable measure of quality is also obtained from $\tilde{R}$ which is an average of the varactor's ability to reflect microwave energy when its bias voltage is swept over a broad range.

[3] W. Shockley, "The theory of *p-n* junctions in semiconductors and *p-n* junction transistors," *Bell Sys. Tech. J.*, vol. 28, p. 435; July, 1949.

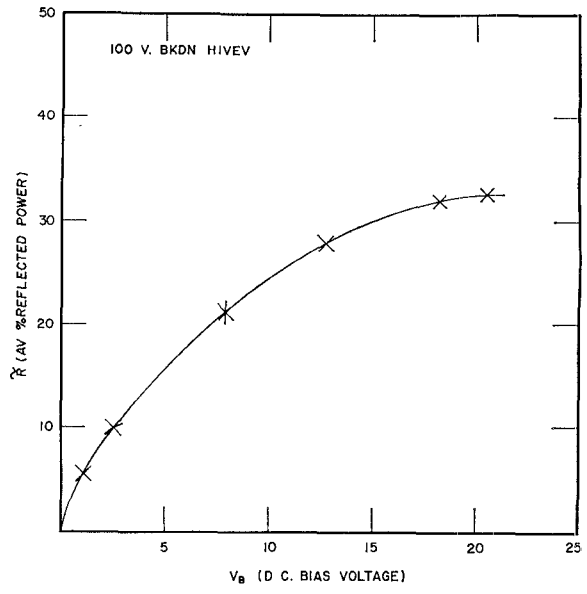

Fig. 5—Average per cent reflected power vs dc bias voltage.

TABLE II
SERIES RESISTANCE OF HIVEV AT VARYING BIAS VOLTAGE MEASURED BY SPM

Diode No.	Capacitance @ zero bias ($\mu\mu$f)	R_s, Series Resistance (ohms)*			
		0–1 v	5–10 v	15–30 v	$\tilde{R}$ (%)
SD-11-C9	0.761	4.9	2.5	1.6	52
SD-11-D9	0.848	12.8	9.1	5.1	47
SD-11-E9	1.832	7.9	4.1	2.4	31
SD-11-G9	3.900	4.4	2.1	1.8	41
SD-11-J9	8.518	5.9	2.3	1.1	21

* 100-v HIVEV. 5–10 v indicates varactor matched at 5-v reverse bias and R_s measured with reactance change due to increase in bias to 10 v.

$\tilde{R}$ is presently submitted as an improved figure of merit for HIVEV. It is a property which can be measured and used as a simple index for correlation with performance in each circuit application. We have measured $\tilde{R}$ for 100-v HIVEV by using a 30-v peak-to-peak sine wave applied relative to a 15-v dc bias. The effect of the amplitude of the sine wave on reflected energy, with dc bias at one half the peak-to-peak value, is shown in Fig. 4. The per cent reflected power does not have an appreciable increase after the bias voltage has been increased to 15 v, consequently this value has been chosen to be a suitable reference bias. Table III gives the typical range observed for $\tilde{R}$ with varactors having 6.5-, 15- and 100-v breakdown using V_B of 2.00-, 5.00- and 15.00-v for standard bias. Table III illustrates the choice of conditions which may be used to compare varactors within a class. The SVM will not overrate a varactor which may have a high cutoff frequency under

TABLE III

TYPICAL RANGE OF AVERAGE PER CENT REFLECTED POWER, $\bar{R}$, BY SVM AND VARACTOR BREAKDOWN VOLTAGE

Range of Zero Bias Capacitance ($\mu\mu$f)	Breakdown Voltage (Volts)	Bias Voltage, V_B* (Volts)	$\bar{R}$ (%)
0.3–2.0	6.5	2.00	25–60
0.5–5	15	5.00	25–60
0.3–5	100	15.0	30–45
5–10	100	15.0	20–30
10–15	100	15.0	10–20

* Sweep Voltage—sine wave at 100 kc, peak-to-peak voltage $2V_B$.

TABLE IV

POWER LEVEL MEASUREMENTS, SVM AND SPM

Incident Power (μw at 9630 Mc)	VSWR* SPM	R† SVM (%)
5	6.4	34
50	6.4	34
100	6.3	34
500	6.1	34
600	6.3	35
700	10.5	36
1000	12.8	38
2000		42
3000		53

* 6.5-v varactor matched at zero bias—1-v reverse bias for reflection.

† 2.00-v bias—4.00-v peak-to-peak sine wave, 100 kc.

moderate reverse voltage but has either a weak capacity-voltage variation or high series resistance near zero bias. Comparison of varactors is accomplished by a process of averaging reflected power over a broad range of bias, hence any defects in a particular region will become evident in the averaging process.

III. SUMMARY

The present paper has described an extension of Houlding's Resonant-Cavity Method for the measurement of the quality of microwave varactors. The Houlding method uses a discrete step in bias to produce a measurable reflected wave whereas the present method uses a swept bias. The method emphasizes the measurement of reflected power as a fundamental variable related to varactor quality. A bench setup for application of the SVM at X band was described. A method for measuring the cutoff frequency of high-Q low breakdown voltage varactors for Parametric Amplifiers was given for the case where the law of capacity vs voltage is known. In this case, it is not necessary to measure capacity or reactance to determine f_c since this quantity is determined by a single measurement of average reflected power $\bar{R}$. This type of measurement was compared with the original method in the case of high-Q silicon mesa varactors and there is satisfactory agreement between the two methods.

The measurement of the quality of high-voltage epitaxial varactors is effected by space-charge layer widening in the epitaxial layer. This effect causes the series resistance external to the p-n junction to be dependent on bias voltage, as demonstrated by calculation and experimental data. A single point measurement of cutoff frequency at large reverse bias may therefore overrate a varactor whose capacity variation is inadequate or whose series resistance near zero bias is excessive. The Sweep-Voltage Method, on the other hand, has the advantage of basing its measurement on the ability of the varactor to reflect microwave power when its bias is swept over a broad range of values. The SVM thereby provides a reliable method for comparison of high-voltage epitaxial varactors, HIVEV, in addition to a convenient method for measuring high-Q varactors.

APPENDIX

Houlding states that the power level for testing varactors should be less than 10^{-5} w.[1] Experience has shown in our laboratory that a considerably higher level of power may be applied to the varactor without effecting the measurement. In order to study the effect of power level on the measured VSWR, a series of measurements were made with varying power level and retuning at zero bias. It was possible to tune the varactor to VSWR of 1.07 or less for power in the range 5 μw to 3 mw. The data in Table IV show measured VSWR vs power level for a typical varactor. There was no significant change in VSWR until the power level was between 600–700 μw. Table IV shows additional data for average per cent reflected power vs power incident on the varactor. In light of these results, 200 μw was chosen as a suitable level for application of the SVM.

ACKNOWLEDGMENT

The varactors used in these studies were developed and produced by the author in conjunction with R. Burchart and C. E. Hail. The measurements were made by D. McArthur.

Excitation of Surface Waves on a Perfectly Conducting Screen Covered with Anisotropic Plasma*

S. R. SESHADRI†, SENIOR MEMBER, IRE

Summary—The field due to a line source of magnetic current situated in a lossless plasma region above a perfectly conducting screen is considered when a uniform static magnetic field is impressed throughout the plasma region parallel to the direction of the line source. It is shown that under certain conditions surface waves are excited on the screen. The dependence of the efficiency of excitation of surface waves on the distance d of the line source from the ground screen is examined. Also, the asymptotic series for the radiation field is derived, and its leading term is shown to vanish for a particular value of d. Under these conditions a strong surface-wave field is maintained near the guiding surface.

Introduction

IN A RECENT PAPER,[1] surface waves were shown to exist on a screen which is assumed to be perfectly conducting in a given direction and completely insulating in the perpendicular direction. In this paper, similar surface waves are shown to exist even when the screen is perfectly conducting provided the medium is anisotropic. Specifically, when a line source of magnetic current is situated in a lossless plasma above a perfectly conducting screen and a uniform static magnetic field is impressed throughout the plasma parallel to the line source, surface waves can exist on the screen. The surface waves are generated only when the plasma is anisotropic and when the operating frequency exceeds the plasma frequency. In addition, for a particular ratio of the operating to the plasma frequency, the static magnetic field must be less than a critical value. The efficiency of excitation of surface waves is evaluated and its dependence on the distance d of the line source from the ground screen is examined for one set of values of plasma and gyromagnetic frequencies. Further, it is shown that by a proper choice of d, it is possible to nullify the leading term in the asymptotic series for the radiation field and thereby obtain a surface wave field which is much stronger than the radiation field near the guiding surface. Similar results have been obtained for the case of surface waves excited by a line source of magnetic current on a dielectric-coated conducting screen.[2]

* Received June 4, 1962; revised manuscript received July 18, 1962. The research reported in this paper was supported by the National Science Foundation Grant NSF 9721.

† Gordon McKay Laboratory, Harvard University, Cambridge, Mass. On leave from Defence Electronics Research Lab., Hyderabad, India.

[1] S. R. Seshadri, "Excitation of surface waves on a unidirectionally conducting screen," IRE TRANS. ON MICROWAVE THEORY AND TECHNIQUES, vol. 10, pp. 279–286; July, 1962.

[2] A. L. Cullen, "The excitation of plane surface waves," *Proc. IEE*, Monograph No. 93R, vol. 101, p. 225; February, 1954.

Excitation of Surface Waves

Consider a perfectly conducting screen of infinite extent located in the x-y plane, where x, y, and z form a right-handed coordinate system. The half space $z>0$ is filled with a uniform plasma. In this investigation, only a primitive model is assumed for the plasma; that is, 1) the plasma as a whole is considered to be at rest, 2) the pressure gradient in the equation of motion is neglected in comparison with the effect of the alternating electric field, 3) the plasma is assumed to be lossless, and 4) the oscillations of the ions are neglected in comparison with those of the electrons.

A line source of magnetic current is located in the plasma at $x=0$, $z=d$; it is parallel to the y axis and may be represented as

$$J_m = \hat{y}\delta(x)\delta(z-d). \tag{1}$$

A uniform magnetic field B_0 is impressed in the y direction throughout the plasma. See Fig. 1. It is desired to examine the electromagnetic field set up by the line source inside the plasma.

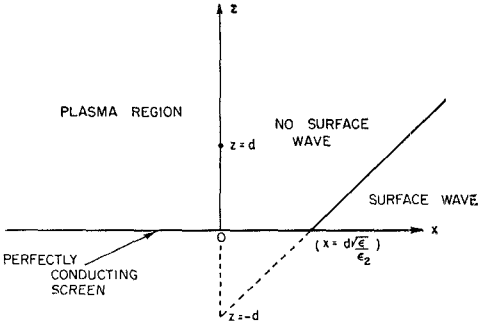

Fig. 1—Geometry of the problem.

As a consequence of the primitive model assumed for the plasma, it is found that in the plasma region ($z>0$), after the usual linearization, the electric and magnetic fields satisfy the time-harmonic Maxwell's equations

$$\nabla \times \boldsymbol{E} = i\omega\mu_0 \boldsymbol{H} - \boldsymbol{J}_m \tag{2a}$$

$$\nabla \times \boldsymbol{H} = -i\omega\epsilon_0 \boldsymbol{\varepsilon} \cdot \boldsymbol{E} \tag{2b}$$

where μ_0 and ϵ_0 are the permeability and dielectric constant pertaining to vacuum. A harmonic time dependence $e^{-i\omega t}$ is assumed for all the field components. The components of the relative dyadic dielectric constant

ϵ are given by the following matrix

$$\epsilon = \begin{bmatrix} \epsilon_1 & 0 & -i\epsilon_2 \\ 0 & \epsilon_3 & 0 \\ i\epsilon_2 & 0 & \epsilon_1 \end{bmatrix} \tag{3}$$

where

$$\epsilon_1 = 1 - \left(\frac{\omega_p}{\omega}\right)^2 \left[1 - \left(\frac{\omega_c}{\omega}\right)^2\right]^{-1}$$

$$\epsilon_2 = \left(\frac{\omega_p}{\omega}\right)^2 \left[\frac{\omega}{\omega_c} - \frac{\omega_c}{\omega}\right]^{-1}$$

and

$$\epsilon_3 = 1 - \left(\frac{\omega_p}{\omega}\right)^2. \tag{4}$$

The plasma frequency ω_p and the gyromagnetic frequency ω_c of the electrons are given by

$$\omega_c = -\frac{eB_0}{m}, \qquad \omega_p{}^2 = \frac{ne^2}{m\epsilon_0} \tag{5}$$

where e is the charge of an electron, m is the mass of an electron, n is the electron density, and B_0 is the applied static magnetic field.

The source and the geometry of the problem are independent of the y coordinate and therefore, all the field quantities are invariant with respect to the y coordinate. With $\partial/\partial y \equiv 0$ in (2), the electromagnetic field is separable into E and H modes which are excited, respectively, by line sources of magnetic and electric current. Since only a line source of magnetic current is present, the H mode is not present; and hence, $E_y = H_x = H_z = 0$. Only a single component of the magnetic field, namely, H_y, is present. It is easily shown with the help of (2b) that the remaining components of the electric field are given by

$$E_x(x, z) = -\frac{i\epsilon_1}{\omega\epsilon_0\epsilon}\frac{\partial}{\partial z}H_y(x, z) - \frac{\epsilon_2}{\omega\epsilon_0\epsilon}\frac{\partial}{\partial x}H_y(x, z)$$

$$E_z(x, z) = \frac{i\epsilon_1}{\omega\epsilon_0\epsilon}\frac{\partial}{\partial x}H_y(x, z) - \frac{\epsilon_2}{\omega\epsilon_0\epsilon}\frac{\partial}{\partial z}H_y(x, z) \tag{6}$$

where

$$\epsilon = \epsilon_1{}^2 - \epsilon_2{}^2. \tag{7}$$

With the help of (2a) and (6) it follows that $H_y(x, z)$ satisfies the following source-dependent wave equation:

$$\left[\frac{\partial^2}{\partial x^2} + \frac{\partial^2}{\partial z^2} + k^2\right] H_y(x, z) = -\frac{i\omega\epsilon_0\epsilon}{\epsilon_1}\delta(x)\delta(z - d) \tag{8}$$

where

$$k^2 = \frac{\omega^2\mu_0\epsilon_0\epsilon}{\epsilon_1} = \frac{k_0{}^2\epsilon}{\epsilon_1}. \tag{9}$$

In (9), k_0 is the wave number corresponding to vacuum. It is assumed in what follows that $\epsilon > 0$. This requirement imposes certain restrictions on the range of values of ω_p/ω and ω_c/ω.

The geometry of the problem suggests the following representations for the field components:

$$H_y(x, z) = \frac{1}{2\pi}\int_{-\infty}^{\infty} \overline{H}_y(\zeta, z)e^{i\zeta x}d\zeta \tag{10a}$$

$$E_x(x, z) = \frac{1}{2\pi}\int_{-\infty}^{\infty} \overline{E}_x(\zeta, z)e^{i\zeta x}d\zeta \tag{10b}$$

and

$$E_z(x, z) = \frac{1}{2\pi}\int_{-\infty}^{\infty} \overline{E}_z(\zeta, z)e^{i\zeta x}d\zeta. \tag{10c}$$

It follows from (6), (8) and (10) that

$$\overline{E}_x(\zeta, z) = -\frac{i\epsilon_1}{\omega\epsilon_0\epsilon}\frac{\partial}{\partial z}\overline{H}_y(\zeta, z) - \frac{i\epsilon_2\zeta}{\omega\epsilon_0\epsilon}\overline{H}_y(\zeta, z), \tag{11a}$$

$$\overline{E}_z(\zeta, z) = -\frac{\epsilon_1\zeta}{\omega\epsilon_0\epsilon}\overline{H}_y(\zeta, z) - \frac{\epsilon_2}{\omega\epsilon_0\epsilon}\frac{\partial}{\partial z}\overline{H}_y(\zeta, z), \tag{11b}$$

and

$$\left[\frac{d^2}{dz^2} + \xi^2\right]\overline{H}_y(\zeta, z) = -\frac{i\omega\epsilon_0\epsilon}{\epsilon_1}\delta(z - d) \tag{12}$$

where

$$\xi = +\sqrt{k^2 - \zeta^2} \qquad k > \zeta$$

$$\xi = +i\sqrt{\zeta^2 - k^2} \qquad k < \zeta. \tag{13}$$

The solution of (12) gives

$$\overline{H}_y(\zeta, z) = \begin{cases} Ae^{i\xi z} + Be^{-i\xi z} & d < z \\ Ce^{i\xi z} + De^{-i\xi z} & d > z \end{cases} \tag{14}$$

and

$$\frac{d}{dz}\overline{H}_y(\zeta, d+) - \frac{d}{dz}\overline{H}^y(\zeta, d-) = -\frac{i\omega\epsilon_0\epsilon}{\epsilon_1}. \tag{15}$$

The radiation condition requires $H_y(x, z)$ to be an outgoing wave for $z \to \infty$; hence $B = 0$. Since the tangential component of the electric field is zero for $z = 0$, it follows from (11a) and (14) that

$$C = R(\zeta)D \quad \text{and} \quad R(\zeta) = \frac{\epsilon_1\xi + i\epsilon_2\zeta}{\epsilon_1\xi - i\epsilon_2\zeta}. \tag{16}$$

The requirement that the tangential component of the magnetic field should be continuous at $z = d$ gives

$$Ae^{i\xi d} = Ce^{i\xi d} + De^{-i\xi d}. \tag{17}$$

The use of the jump condition (15) in (14) leads to

$$Ae^{i\xi d} - (Ce^{i\xi d} - De^{-i\xi d}) = -\frac{\omega\epsilon_0\epsilon}{\epsilon_1\xi}. \tag{18}$$

The expressions for A, C and D may be obtained from the solution of the simultaneous equations (16), (17) and (18). The results are:

$$A = -\frac{\omega\epsilon_0\epsilon}{2\epsilon_1\xi}\left[e^{-i\xi d} + R(\zeta)e^{i\xi d}\right],$$

$$B = 0,$$

$$C = -\frac{\omega\epsilon_0\epsilon}{2\epsilon_1\xi}R(\zeta)e^{i\xi d},$$

$$D = -\frac{\omega\epsilon_0\epsilon}{2\epsilon_1\xi}e^{i\xi d}. \tag{19}$$

The substitution of (14) (10a) and the use of (16) and (19) yields

$$H_y(x, z) = \frac{1}{2\pi}\int_{-\infty}^{\infty} -\frac{\omega\epsilon_0\epsilon}{2\epsilon_1\xi}\left[e^{-i\xi d} + \frac{\epsilon_1\xi + i\epsilon_2\zeta}{\epsilon_1\xi - i\epsilon_2\zeta}e^{i\xi d}\right] \cdot e^{i\zeta x + i\xi z}d\zeta \qquad \text{for } z > d. \tag{20a}$$

$$H_y(x, z) = \frac{1}{2\pi}\int_{-\infty}^{\infty} -\frac{\omega\epsilon_0\epsilon}{2\epsilon_1\xi}\left[e^{-i\xi z} + \frac{\epsilon_1\xi + i\epsilon_2\zeta}{\epsilon_1\xi - i\epsilon_2\zeta}e^{i\xi z}\right] \cdot e^{i\zeta x + i\xi d}d\zeta \qquad \text{for } z < d. \tag{20b}$$

The contour for the integrals in (20a) and (20b) is along the real axis in the ζ plane as shown in Fig. 2. The integrand in (20a) and (20b) has a pole at

$$\zeta = +\frac{k\epsilon_1}{\sqrt{\epsilon}} = +k_0\sqrt{\epsilon_1}.$$

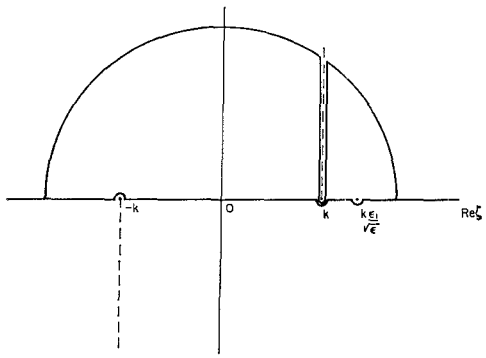

Fig. 2—Contour of integration in the ζ plane

This pole is either on the real or the imaginary axis, depending upon whether ϵ_1 is positive or negative. Since the aim of this paper is to examine the characteristics of the surface wave that is excited on the ground screen, only positive values of ϵ_1 are considered. This leads to the following restrictions:

1) $\frac{\omega_p}{\omega} < 1$ and

2) $-\left[1 - \left(\frac{\omega_p}{\omega}\right)^2\right]^{1/2} < \frac{\omega_c}{\omega} < \left[1 - \left(\frac{\omega_p}{\omega}\right)^2\right]^{1/2}$.

For $0 < \epsilon_1 < 1$, the pole of the integrand is on the real axis and the contour of integration is indented above the singularity $-k$ and below the singularities at k and $k\epsilon_1/\sqrt{\epsilon}$. For $x > 0$, the integrals may be evaluated by closing the contour in the upper half of the ζ plane as shown in Fig. 2. The contribution to the integrals in (20a) and (20b) is the sum of the residue at the pole $\zeta = k\epsilon_1/\sqrt{\epsilon}$ and a branch-cut integral.

The value of the branch-cut integral depends on some inverse power of x. Hence, for sufficiently large x, the value is negligible compared to the contribution due to the pole. Thus, for positive large x,

$$H_y(x, z) = -\omega\epsilon_0|\epsilon_2| \exp\left\{\frac{ik\epsilon_1}{\sqrt{\epsilon}}x - \frac{k|\epsilon_2|}{\sqrt{\epsilon}}(z + d)\right\}$$

$$= -\omega\epsilon_0|\epsilon_2| \exp\left\{ik_0\sqrt{\epsilon_1}\,x - \frac{k_0|\epsilon_2|}{\sqrt{\epsilon_1}}(z + d)\right\}. \tag{21}$$

It is obvious that $H_y(x, z)$ given in (21) represents a surface wave propagating in the positive x direction and exponentially attenuated in the z direction. The phase velocity v_p of the wave is given by

$$v_p = \frac{c_0}{\sqrt{\epsilon_1}} = \frac{c\sqrt{\epsilon}}{\sqrt{\epsilon_1}} \tag{22}$$

where c_0 and c are, respectively, the velocity of propagation of electro-magnetic waves in vacuum and in an unbounded anisotropic plasma. Since $\epsilon_1 < 1$, the phase velocity of the surface wave is greater than the velocity of electromagnetic waves in vacuum and less than that in the unbounded anisotropic plasma. When the static magnetic field is reversed in direction, ϵ_2 changes sign and the pole of the integrand in (20a) and (20b) occurs now at $\zeta = -k\epsilon_1/\sqrt{\epsilon} = -k_0\sqrt{\epsilon_1}$. Hence, the surface wave reverses direction and propagates in the negative x direction, instead of in the positive x direction as described in (21). When there is no static magnetic field, ϵ_2 vanishes and from (20a) and (20b) it is clear that, in this case, there is no surface wave. This means that besides other restrictions the plasma must be anisotropic if surface waves are to exist on the ground screen.

The substitution of (21) in (6) gives the other field components of the surface wave as follows:

$$E_x(x, z) = 0$$

$$E_z(x, z) = \frac{k|\epsilon_2|}{\sqrt{\epsilon}} \exp\left\{\frac{ik\epsilon_1}{\sqrt{\epsilon}}x - \frac{k|\epsilon_2|}{\sqrt{\epsilon}}(z + d)\right\}. \tag{23}$$

Therefore, the surface wave is a TEM wave with respect to the direction of propagation.

In the integral representation (20a) and (20b) for $H_y(x, z)$, the first term corresponds to the incident field due to the line source and the second term corresponds to the field of the line source reflected from the

ground screen. The asymptotic form of the reflected field is obtained by performing a saddle-point evaluation of the integral (20a) and (20b). For this purpose, the transformation

$$\zeta = k \cos \tau \tag{24}$$

is introduced. With it, the expression [(20a) and (20b)] for $H_y(x, z)$ becomes

$$H_y(x, z) = H_y^i(x, z) + H_y^r(x, z)$$

where

$$H_y^i(x, z) = \frac{1}{2\pi} \int_C \frac{\omega\epsilon_0\epsilon}{2\epsilon_1} e^{ik[x \cos \tau + |z-d| \sin \tau]} d\tau \tag{26}$$

$$H_y^r(x, z) = \frac{1}{2\pi} \int_C \frac{\omega\epsilon_0\epsilon}{2\epsilon_1} \frac{\epsilon_1 \sin \tau + i\epsilon_2 \cos \tau}{\epsilon_1 \sin \tau - i\epsilon_2 \cos \tau} \cdot e^{ik[x \cos \tau + (z+d) \sin \tau]} d\tau. \tag{27}$$

The original contour along the real axis in the ζ plane is transformed into the contour C shown in Fig. 3. The asymptotic form of the reflected field is obtained by a saddle-point evaluation of the integral in (27). The saddle point which lies in the interval $0 < \tau_0 < \pi$ is given by

$$\tau_0 = \tan^{-1} \frac{z + d}{|x|}. \tag{28}$$

Setting $\tau = \tau_1 + i\tau_2$, the equation of the saddle-point contour is easily shown to be given by

$$\tau_1 = \tau_0 \mp \cos^{-1} (\operatorname{sech} \tau_2) \quad \text{for} \quad \tau_2 \gtrless 0. \tag{29}$$

The pole of the integrand in (27) is seen to occur at $P: \tau_1 = 0$, $\tau_2 = \cosh^{-1}(\epsilon_1/\sqrt{\epsilon})$. For $x = 0$, $\tau_0 = \pi/2$ and for this case, the contour C can be deformed into the saddle-point contour without crossing the pole. On the other hand, for $x = \infty$ $\tau_0 = 0$, and the original contour C crosses the pole P, and the residue of the integral at this pole must be added to the contribution from the saddle point. The saddle contour corresponding to the saddle point

$$\tau_0(P) = \cos^{-1} \frac{\epsilon}{\sqrt{\epsilon_1}} \tag{30}$$

is seen to pass through the pole P. If $\tau_0 < \tau_0(P)$, the pole is crossed and the surface wave occurs; if $\tau_0 > \tau_0(P)$, there is no surface wave. Thus the region of physical space where the surface wave is present is obtained from (28), (30) and (7):

$$z + d < \frac{\epsilon_2}{\sqrt{\epsilon}} x. \tag{31}$$

The region of the physical space where the surface wave is present is shown in Fig. 1. If the impressed static field is zero, $\epsilon_2 = 0$. From (31) and Fig. 1, it is seen then that there is no region where the surface wave exists.

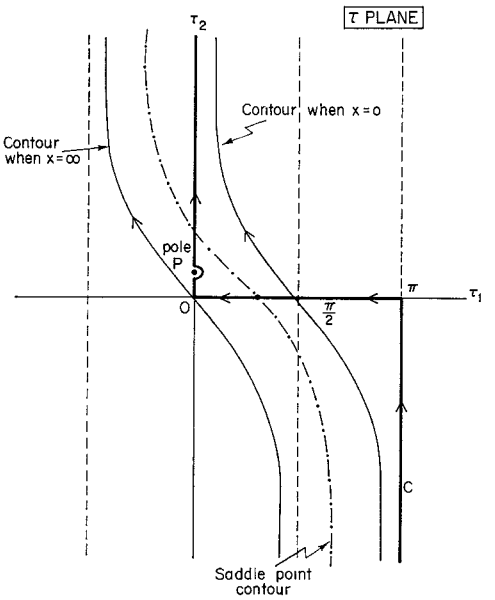

Fig. 3—Integration countours in the τ plane, $x > 0$.

Radiation Pattern

In order to obtain the radiation pattern, it is necessary to evaluate the integrals in (26) and (27) asymptotically. For this purpose, let

$$x = \rho \cos \theta; \qquad z = \rho \sin \theta. \tag{32}$$

With (32), (26) and (27) may be rewritten as

$$H_y^i(x, z) = \frac{1}{2\pi} \int \frac{\omega\epsilon_0\epsilon}{2\epsilon_1} e^{-ikd \sin \tau} e^{ik\rho \cos (\theta - \tau)} d\tau \text{ for } z > d \tag{33}$$

and

$$H_y^r(x, z) = \frac{1}{2\pi} \int \frac{\omega\epsilon_0\epsilon}{2\epsilon_1} \frac{\epsilon_1 \sin \tau + i\epsilon_2 \cos \tau}{\epsilon_1 \sin \tau - i\epsilon_2 \cos \tau} \cdot e^{ikd \sin \tau} e^{ik\rho \cos (\theta - \tau)} d\tau. \tag{34}$$

For $k\rho \gg 1$, (33) and (34) are easily evaluated asymptotically with the result that

$$H_y(x, z) = H_y^i(x, z) + H_y^r(x, z) = \frac{\omega\epsilon_0\epsilon}{2\epsilon_1} \frac{e^{i(k\rho - \pi/4)}}{\sqrt{2\pi k\rho}} \cdot \left[e^{-ikd \sin \theta} + \frac{\epsilon_1 \sin \theta + i\epsilon_2 \cos \theta}{\epsilon_1 \sin \theta - i\epsilon_2 \cos \theta} e^{ikd \sin \theta} \right]. \tag{35}$$

With (6) and (32), it may easily be shown that for $k\rho \gg 1$,

$$E_\theta(\rho, \theta) \simeq - \frac{\epsilon_1 k}{\omega\epsilon_0\epsilon} H_y(\rho, \theta). \tag{36}$$

The outward power flow, per unit area, per unit length of the screen at an angle θ is obtained from (35) and

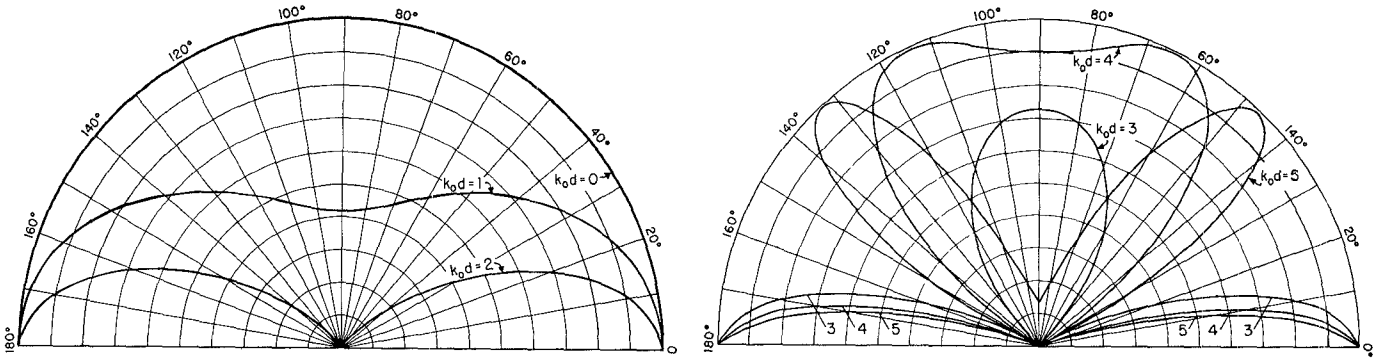

(a) (b)

Fig. 4—Radiation pattern $\omega_p/\omega=0.5$, $\omega_c/\omega=0$.

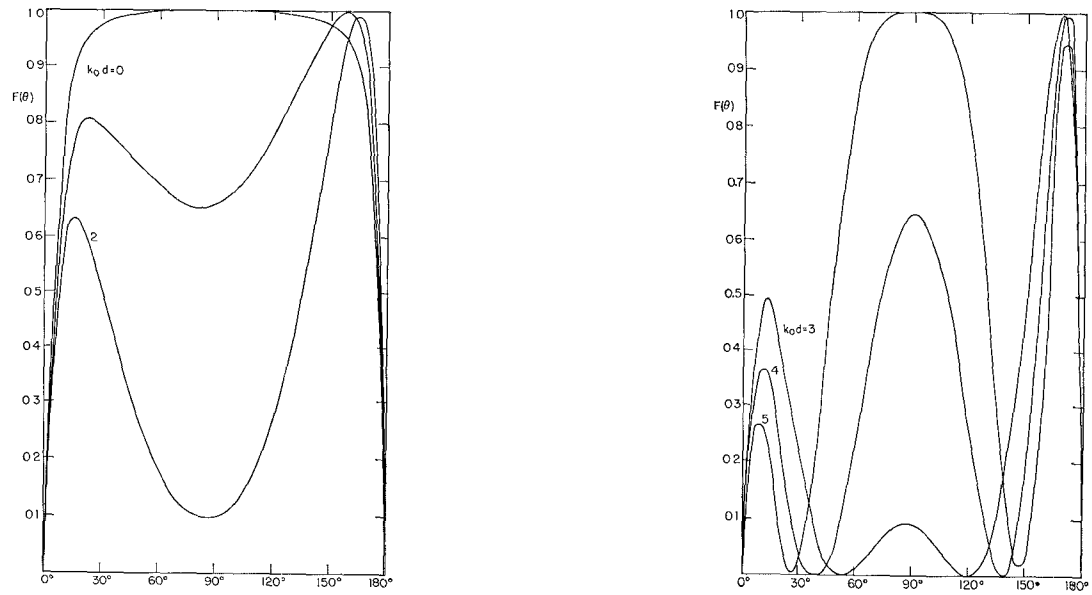

(a) (b)

Fig. 5—Radiation pattern $\omega_p/\omega=0.5$, $\omega_c/\omega=0.25$.

(36) to be

$$S=\frac{1}{2}\operatorname{Re}\hat{\rho}\cdot\boldsymbol{E}(\rho,\theta)\times\boldsymbol{H}^*(\rho,\theta)=\frac{k\epsilon_1}{2\omega\epsilon_0\epsilon}\mid H_y(\rho,\theta)\mid^2$$

$$=\frac{\omega\epsilon_0\epsilon}{8\pi\epsilon_1\rho}F(\theta) \tag{37}$$

where

$$F(\theta)=\frac{[\epsilon_1\sin\theta\cos(kd\sin\theta)-\epsilon_2\cos\theta\sin(kd\sin\theta)]^2}{[\epsilon\sin^2\theta+\epsilon_2{}^2]}. \tag{38}$$

$F(\theta)$ given in (38) is defined to be the radiation pattern.

In Figs. 4 and 5, the radiation pattern $F(\theta)$ is plotted for two different sets of values of ω_p/ω and ω_c/ω. In each figure, k_0d is used as a parameter. The patterns are symmetrical about $\theta=\pi/2$, when $\omega_c/\omega=0$. When $\omega_c/\omega\neq0$, the plasma is anisotropic and the patterns are no longer symmetrical about $\theta=\pi/2$. A reversal in the direction of the magnetic field changes the sign of ϵ_2 and hence causes the radiation pattern to be rotated through 180° about the z axis.

Efficiency of Excitation

The efficiency of excitation of surface waves is defined to be the ratio of the power propagated as a surface wave per unit width of the screen to the sum of the powers in the surface wave and the radiation fields. The power per unit width of the screen P_R delivered by the magnetic current line source to the radiation field is easily seen to be given by

$$P_R=\int_0^\pi S\rho d\theta=\frac{\omega\epsilon_0\epsilon}{8\pi\epsilon_1}\int_0^\pi F(\theta)d\theta. \tag{39}$$

The power in the surface wave per unit width of the screen is obtained from the relation

$$P_S=\int_0^\infty\hat{x}\cdot\frac{1}{2}\operatorname{Re}\boldsymbol{E}(x,z)\times\boldsymbol{H}^*(x,z)dz, \tag{40}$$

where $\boldsymbol{H}(x,z)$ and $\boldsymbol{E}(x,z)$ are given, respectively, in (21) and (23). The substitution of $\boldsymbol{E}(x,z)$ and $\boldsymbol{H}(x,z)$

from (23) and (21) in (40) gives

$$P_S = \tfrac{1}{4}\omega\epsilon_0 \left| \epsilon_2 \right| e^{-2kd(|\epsilon_2|/\sqrt{\epsilon})}. \tag{41}$$

The efficiency of excitation obtained from (39) and (41) is

$$\eta = \frac{P_S}{P_S + P_R} = \frac{e^{-2k_0 d(|\epsilon_2|/\sqrt{\epsilon_1})}}{e^{-2k_0 d(|\epsilon_2|/\sqrt{\epsilon})} + \dfrac{\epsilon}{2\pi\epsilon_1 \left| \epsilon_2 \right|} \displaystyle\int_0^\pi F(\theta)d\theta}. \tag{42}$$

When $k_0 d = 0$, $\int_0^x F(\theta)d\theta$ can easily be evaluated and an explicit expression obtained for η. From (38), for $k_0 d = 0$, it is seen that

$$F(\theta) = \frac{\epsilon_1^2 \sin^2\theta}{[\epsilon \sin^2\theta + \epsilon_2^2]}. \tag{43}$$

It is readily shown that for $F(\theta)$ given in (43)

$$\int_0^\pi F(\theta)d\theta = \frac{\pi\epsilon_1}{\epsilon}(\epsilon_1 - \left| \epsilon_2 \right|). \tag{44}$$

The substitution of (44) in (42) yields the following result for $k_0 d = 0$:

$$\eta = \left[\frac{1}{2} + \frac{\epsilon_1}{2\left| \epsilon_2 \right|}\right]^{-1}. \tag{45}$$

From (45) and (4), it is obvious that for $k_0 d = 0$, the efficiency of excitation η increases as ω_c/ω increases.

For other values of $k_0 d$, the value of

$$\int_0^\pi F(\theta)d\theta$$

has to be obtained by numerical integration and the value of η is then determined from (42). For one set of values of ω_p/ω and ω_c/ω, the values of η are given in Table I for different values of $k_0 d$. It is found that the

TABLE I

VALUES OF η FOR $\omega_p/\omega = 0.5$ AND $\omega_c/\omega = 0.25$

$k_0 d$	0	1	2	3	4	5
η	0.17	0.17	0.25	0.31	0.23	0.13

maximum value of η does not occur when $d = 0$, but at some other value of d. Hence, it follows that by a suitable adjustment of the distance of the line source from the ground screen, the power delivered to the radiation field may be minimized and a maximum value obtained for the efficiency of excitation.

Approximate Evaluation of $H_y(x, z)$

The integral representation of $H_y(x, z)$ given in (20a) and (20b) shows that the contribution to $H_y(x,z)$ arises from a pole and a branch-cut integral. The residue at the pole $\zeta = k\epsilon_1/\sqrt{\epsilon}$ gives the surface-wave field and this has been evaluated before. It is now desired to obtain the contribution from the branch-cut integral. This contribution can be obtained as a series in inverse powers of x by expanding the integrand in a Taylor series and integrating term by term. The result of a straightforward calculation gives

$$H_y(x, z) = \frac{k\omega\epsilon_0\epsilon}{\sqrt{2\pi}\,\epsilon_2} e^{i(kx-\pi/4)}\left[\frac{F_1(z, d)}{(kx)^{3/2}} - \frac{3F_2(z, d)}{8(kx)^{5/2}}\right] \tag{46}$$

where

$$F_1(z, d) = z + d - \frac{\epsilon_2}{\epsilon_1} dzk - \frac{\epsilon_1}{\epsilon_2 k} \tag{47}$$

and

$$F_2(z, d) = \frac{7}{k}\left(\frac{\epsilon_1}{\epsilon_2}\right) - \frac{8}{k}\left(\frac{\epsilon_1}{\epsilon_2}\right)^3 + \left[8\left(\frac{\epsilon_1}{\epsilon_2}\right)^2 - 3\right](z + d) - \frac{\epsilon_2}{\epsilon_1} kdz - 4k\frac{\epsilon_1}{\epsilon_2}(d + z)^2 - \frac{4k^2}{3}(d + z)^2 - \frac{4}{3}\frac{\epsilon_2}{\epsilon_1} k^3 dz(d^2 + z^2). \tag{48}$$

The conditions for validity of the asymptotic series in (46) are

$$x \gg d + z; \qquad kx \gg \frac{\epsilon}{\epsilon_2^2}. \tag{49}$$

Observe that (20a) and (20b) and the condition equation (49) are symmetrical in z and d. It follows that (46) is valid for $z > d$ or $z < d$.

The asymptotic series in (46) represents the radiation field. If the height d of the line source from the ground screen is such that $d = d_m = \epsilon_1/\epsilon_2 k$, then it follows that $F_1(z, d_m) = 0$ and

$$H_y(x, z) = -\frac{3k\omega\epsilon_0\epsilon}{8\sqrt{2\pi}\,\epsilon_2} F_2(z, d_m) \frac{e^{i(kx-\pi/4)}}{(kx)^{5/2}}, \tag{50}$$

where

$$F_2(z, d_m) = 4\left[1 - \frac{2}{3}\left(\frac{\epsilon_1}{\epsilon_2}\right)^2\right]\left[\frac{1}{k}\left(\frac{\epsilon_1}{\epsilon_2}\right) - z\right]. \tag{51}$$

If the line source is at a distance d_m from the ground screen, the first term in the asymptotic expansion of the radiation field vanishes and the radiation field near the ground screen becomes very weak. An almost pure surface wave may be said to be generated in this special case. This situation is similar to that observed by Cullen in his treatment of the excitation of surface waves on a reactive surface.

Acknowledgment

The author wishes to thank Profs. R. W. P. King and T. T. Wu for their help and encouragement with this research.